ISSN 1392-2114 ULTRAGARSAS, Nr.1(38). 2001.

General theory for quantative evaluation of three - dimentional vibrations from time-average holographic interferograms

A. Palevičius

Kaunas Atžalynas Secondary School
Partizanu g. 46, LT-3009 Kaunas

Introduction

A procedure for calculating the amplitudes of the normal and tangential components of the displacement vector of three-dimensional vibrations of any point on the surface of mechanical wave system is proposed on the basis of experimental holographic interfrometry data and the theory of vibrations of mechanical systems

The problem of determination the amplitude – frequency response characteristics of a vibrating surface, which vibrates in three dimensions in the majority of cases, is encountered in the analysis of vibrations of mechanical system. The development of methods for calculating the characteristics of three – dimensional (3D) vibrations contributes to the solution of vital problems in the investigation, design, testing, and diagnostics of systems.

There are publications devoted to evaluation of deformation vector and quantitive analysis of holographic particle data in [1-11]. The papers give an instrument for interpretation and calculation component of vector deformation surface of solid bodies of the simple shapes and the use for complex forms of the links is not directly available and need to modified it. The problem is that procedure and algorithms must include into calculation relations between vibrations type and the geometry of the shapes of links. The 3-D vibrations for wave mechanical system shapes of links take part in the analysis process and its enable to find algorithms and common methods of investigation [12-15].

In the present paper a method is described for calculation of the amplitudes of the normal and tangential components of the displacement vector of 3D vibrations of the surface of deformable elements on the basis of experimental holographic-interferometry data and the theory of vibrations of mechanical systems. In contrast with previous publication on this topic, the proposed method permits a severalfold reduction in the quantity of input data for analysis of vibrations from holographic interferograms.

Algorithm calculation 3-D vibration of the links mechanical systems

We now discuss the essentials of the method [16, 17].

A point ***i*** is given on the surface of a vibrating link of system (see Fig. 1), and the displacement vector of the 3D vibrations of this point is written in the form

$$\overline{\mathbf{R}}_i(t) = U_i(t)\hat{\mathbf{i}} + V_i(t)\hat{\mathbf{j}} + W_i(t)\hat{\mathbf{k}}. \qquad (1)$$

We represent the components of the vector $\boldsymbol{R_i(t)}$ at the ***i***-th point in the form

$$\begin{aligned} U(t) &= U_0^i \cos(\omega t + a_i), \\ V(t) &= V_0^i \cos(\omega t + \beta_i), \\ W(t) &= W_0^i \cos(\omega t + \gamma_i), \end{aligned} \qquad (2)$$

where $\boldsymbol{U_0^i}$, $\boldsymbol{V_0^i}$, and $\boldsymbol{W_0^i}$ are the amplitudes of forced vibrations of the i-th point along the *z, t,* and *r* coordinate axes respectively.

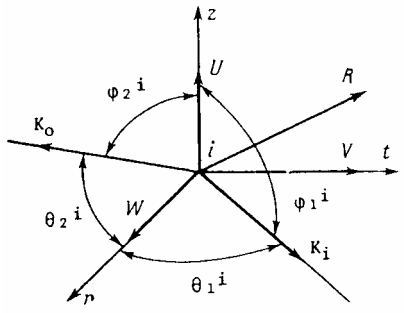

Fig. 1. **Diagram for interpretation of measurements of vibrations. The scheme of optical measurement of vibrations of point *i*: *r, t, z* is of the orthogonal system of coordinates, *R* is the vector of spatial vibrations of the *i* –th point of the surface, *U, V, W* are the components of the vector of spatial vibrations of the *i* -th point in the directions of the coordinate axis *r, t, z* correspondingly, $\hat{K}_i$ is the unit vector of lightening of point *i*, $\hat{K}_0$ is the unit vector of observation of point *i*, θ_1', θ_2' are the angles of unit vectors of lightening and observation with the coordinate axis *r* correspondingly, φ_1^i, φ_2^i are the angles between the coordinate axis *z* and the unit vectors of lightening and observation correspondingly**

The amplitudes of forced vibrations of points of a solid are determined approximately by expanding the models of vibration with respect to *k*. With this in mind, we express $\boldsymbol{U_0^i}$, $\boldsymbol{V_0^i}$, and $\boldsymbol{W_0^i}$ as follows [18]:

$$U_0^i = \sum_1^k A_j^u F_{ij}^u;\ V_0^i = \sum_1^k A_j^v F_{ij}^v;$$

$$W_0^i = \sum_1^k A_j^w F_{ij}^w; \qquad j = 1,2,...,k, \qquad (3)$$

where $\boldsymbol{F_{ij}}$ is the value of the *j*-th mode for the i-th point, $\boldsymbol{Aj}$ is the coefficient of influence of the *j*-th mode, and **k** is number of modes analyzed.

Consequently, in order to calculate the component of 3D vibration vector, it is necessary to determine the values of F_{ij}^{u}, F_{ij}^{v}, F_{ij}^{w}, A_j^{u}, A_j^{v}, A_j^{w}, α_i, β_i, γ_I.

The amplitudes of the first k modes can be calculated according to previously presented analytical expressions for modes of vibration, with allowance for the geometry of investigated links and its attachment boundary conditions.

We consider determination of $A_j^{u}, A_j^{v}, A_j^{w}, \alpha_i, \beta_i, \gamma_I$ on the basis-of holographic interferometry data. We refer to Fig. 1. We denote the unit vector in the direction of observation of point i by K_o, and the unit vector in the direction opposite to the direction of illumination by K_i the sensitivity vector K [18] can be written in the form

$$\overline{\mathbf{K}} = \hat{\mathbf{K}}_i + \hat{\mathbf{K}}_0 . \tag{4}$$

Or, in terms of the components in the basis (**z, t, r**),

$$\overline{\mathbf{K}}^i = K_r^i \hat{\mathbf{r}} + K_t^i \hat{\mathbf{t}} + K_z^i \hat{\mathbf{z}}, \tag{5}$$

where K_r^i, K_t^i, and K_z^i are the projections of the sensitivity vector on to the **r**, **t**, and **z** axes.

The projections K_r^i, K_t^i, and K_z^i of the sensitivity vector K can be expressed in terms of trigonometric functions of the angles θ_1, θ_2, φ_1, φ_2 formed by the unit vectors K_i and K_o with r and z axes according to the relations

$$\begin{aligned} K_z^i &= \cos\varphi_2^i + \cos\varphi_1^i, \\ K_t^i &= \sin\theta_1^i \sin\varphi_1^i - \sin\theta_2^i \sin\varphi_2^i, \\ K_r^i &= \cos\theta_1^i \sin\varphi_1^i + \cos\theta_2^i \sin\varphi_2^i . \end{aligned} \tag{6}$$

The phase variation in the transmission of light from the source to point I on the surface of the deformable link and back to the holographic interferogram as a result of the surface vibrations is [19]

$$\Omega = \frac{2\pi}{\lambda} \overline{\mathbf{R}}_i(t) \overline{\mathbf{K}}^i, \tag{7}$$

where λ is the emission wavelength of the laser used to record the holographic interferograms.

Substituting the scalar product of the 3D vibration vector and sensitivity vector in Eq.7, we obtain

$$\Omega = \frac{2\pi}{\lambda} \left[U(t) K_z^i + V(t) K_t^i + W(t) K_r^i \right]. \tag{8}$$

The characteristic distribution function of the interference fringes on the surface of the investigated link in the case of time averaging in harmonic excitation is given by [20]:

$$X_\Phi(\Omega) = \frac{1}{T} \int_0^T \exp(i\Omega) dt. \tag{9}$$

Substituting Eq. 8 in 9 and taking Eq. 2 and 3 into account, we have

$$X_\Phi(\Omega) = \frac{1}{T} \int_0^T \exp[in(\Omega_1 \cos\omega t - \Omega_2 \sin\omega t)] dt, \tag{10}$$

where n is the wave number, which is defined as $n=2\pi/\lambda$;

$$\Omega_1 = U_0^i \cos\alpha_i K_z^i + V_0^i \cos\beta_i K_t^i + W_0^i \cos\gamma_i K_r^i,$$

$$\Omega_2 = U_0^i \sin\alpha_i K_z^i + V_0^i \sin\beta_i K_t^i + W_0^i \sin\gamma_i K_r^i . \tag{11}$$

We use this result to write the characteristic distribution function of the interference fringes on the surface of the deformable link in the form [19]:

$$X_f(\Omega) = J_o[n(\Omega_1 + \Omega_2)]^{1/2}.$$

Comparing the arguments of the function with allowance for Eq.11, we obtain a nonlinear algebraic equation for the components $A_j^{u}, A_j^{v}, A_j^{w}, \alpha_i, \beta_i, \gamma_I$:

$$\begin{aligned} \frac{\Omega^i \lambda^2}{4\pi} = &\left[\left(\sum_1^k A_j^{\varpi} F_{ij}^{\varpi} \right) \cos\gamma_i K_r^i + \left(\sum_1^k A_j^{v} F_{ij}^{v} \right) \cos\beta_i K_t^i + \right. \\ &\left. + \left(\sum_1^k A_j^{u} F_{ij}^{u} \right) \cos\alpha_i K_z^i \right]^2 + \left[\left(\sum_1^k A_j^{\varpi} F_{ij}^{\varpi} \right) \sin\gamma_i K_r^i + \right. \\ &\left. + \left(\sum_1^k A_j^{v} F_{ij}^{v} \right) \sin\beta_1 K_t^i + \left(\sum_1^k A_j^{u} F_{ij}^{u} \right) \sin\alpha_i K_z^i \right]^2 . \end{aligned} \tag{12}$$

The known quantities are Ω, which are calculated [19] at the centers of the dark interference fringes from holographic interferograms of deformable link according to Eq. 7:

$$\Omega_p = (p - 0{,}25)\pi + 0{,}125 / \pi(p - 0{,}25), \tag{13}$$

where p is the fringe order on the holographic interferogram with the I th point at its center, measured from the brightest nodal line; K_r^i, K_t^i, and K_z^i are calculated according to Eq. 6, F_{ij}^{u}, F_{ij}^{v}, F_{ij}^{w} are calculated from analytical equation for the normal vibrational modes of link as a function of their geometry and design characteristics.

We use a procedure decribed in [21] to solve the nonlinear Eq. 12. Several holographic interferograms must be obtained for different angles of illumination and observation of the investigated transducer in order to determine the unknowns in the problem. Making use of Eq.12, we determine the discrepancies resulting from experimental errors to the equation

$$\begin{aligned} f_i = &\left[\left(\sum_1^k A_j^{u} F_{ij}^{u} \right) \cos\alpha_1 K_z^i + \left(\sum_1^k A_j^{v} F_{ij}^{v} \right) \cos\beta_1 K_t^i + \right. \\ &\left. + \left(\sum_1^k A_j^{\varpi} F_{ij}^{\varpi} \right) \cos\gamma_i K_r^i \right]^2 - \left[\left(\sum_1^k A_j^{u} F_{ij}^{u} \right) \sin\alpha_i K_z^i + \right. \\ &\left. + \left(\sum_1^k A_j^{v} F_{ij}^{v} \right) \sin\beta_i K_t^i + \right. \\ &\left. + \left(\sum_1^k A_j^{\varpi} F_{ij}^{\varpi} \right) \sin\gamma_i K_r^i \right] - \left[\frac{\Omega_i}{n} \right]. \end{aligned} \tag{14}$$

We differentiate this equation with respect to the unknown components of Eq. 12 and form a matrix G with columns

$$G_j^{(i)} = \frac{\partial f_i}{\partial A_j^u};\ G_{j+k}^{i} = \frac{\partial f_i}{\partial A_j^v};\ G_{j+2k} = \frac{\partial f_i}{\partial A_j^{\varpi}};$$

$$G_{1+3k}^{(i)} = \frac{\partial f_i}{\partial \alpha_i};$$

$$G_{2+3k} = \frac{\partial f_i}{\partial \beta_i};\ G_{3+3k} = \frac{\partial f_i}{\partial \gamma_i}.\ j = 1,2...,k; \qquad (15)$$

If q holographic interferograms are recorded for the I – th point in different directions of illumination and observation, and if q sets of data are formed from the results, G is a q x $36(2k+3)$ matrix.

For an arbitrarily specified vector of unknowns

$$B_{\mathrm{H}} = \begin{bmatrix} A_1^u, A_2^u, ..., A_k^u, A_1^v, A_2^v, . \\ .., A_k^v, A_1^{\varpi}, A_2^{\varpi}, ..., A_k^{\varpi}, \alpha, \beta, \gamma \end{bmatrix}. \qquad (16)$$

We seek solutions by iteration in the form $\sigma = \Gamma^{-1}\boldsymbol{p}$:

$$\Gamma_{ij} = \sum_1^q G_i^{(i)} G_j^{(i)};\ P_j = -\sum_1^q f_i G_j^{(i)},$$

$$j = 1,2...,(3+3k). \qquad (17)$$

We have calculated the vibrations of a link of mechanical system the basis of the proposed method. We obtained several holograms with different directions of the sensitivity vector relative to the normal to the link surface.

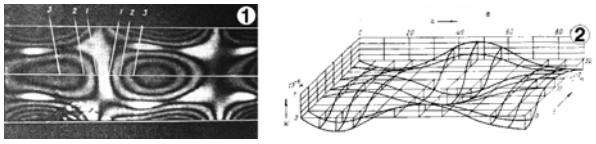

Fig. 2. **Holographic interferograms of the vibrations of a piezoceramic plate: 1 - frequency of vibration plate 45,8 kHz; the sensivity is directed along the normal to the plate surface; 2 - amplitude distribution of vibrations normal to the surface of the plate.**

Fig. 2. shows a holographic interferogram with the sensitivity vector directed along the normal to link surface. The values of the angles during recording of the holographic interferogram were $\theta_1 = \theta_2 = 0^{\mathrm{o}}$, $\varphi_1 = \varphi_2 = 90^{\mathrm{o}}$. Substituding the values of the angles in Eq. 6, we calculate the components of the sensitivity vector $\boldsymbol{K_r^i}$, $\boldsymbol{K_t^i}$, and $\boldsymbol{K_z^i}$. The variation of the phase Ω is determined from the holographic interferogram by means of Eq. 3. We find the brightest fringe on the view plane of the holographic interferogram, i.e., the so-called nodal fringe. For example, the orders of the dark fringes in Fig. 2. for the given points 1 –3 are p = 1, 2, 3, respectively; they differ in sign on either side of the nodal fringe, since the displacements are in oposite directions. We substitute these values to Eq. 13 and calculate Ω. Analytical equations for the calculation of $\boldsymbol{F_{ij}^u}$, $\boldsymbol{F_{ij}^v}$, $\boldsymbol{F_{ij}^w}$ are given in [19].

Calculation of sensitivity vector components

It is necessary for calculation of the normal and tangential components of the three-dimentional oscillation vector of members of mechanical systems to determine projections of the sensitivity vectors [16].

It is suggested to perform calculation of projections of the sensitivity vector directly from image of a holographic interferogram. In order to do this, we shall use Fig. 1. This diagram illustrates the connection between the optical train of the holographic test rig and the measured point lying on the surface of the studies member. On the surface of the member the point M is considered, which vector of three-dimentional oscillations is presented by tangential $\overline{U}$, $\overline{V}$ of normal $\overline{W}$ components in the orthogonal basis $\vec{i}, \vec{j}, \vec{k}$ corresponding to directions of coordinate axes *z, t, r*. The connection of the measured point of the member with the holographic test rig is determined via vector $\hat{K}_i$ which gives the direction of observation of the investigated point of the member.

Position of vectors $\hat{K}_i, \hat{K}_0$ in space are determined by angles θ_1, θ_2, ψ_1, ψ_2, φ_1, φ_2, which form vectors with the coordinates axes *z, t, r* (Fig 1).

In order to calculate the projections K_r, K_t, K_z of the sensitivity vector by expressions (6), it is necessary to determine the angles θ_1, θ_2, φ_1, φ_2. Usually the angles θ_1, θ_2, φ_1, φ_2 were determined experimentally from the geometry of the optical of holographic train, which causes errors. Here we propose a procedure which allows the determination of these angles directly from image of the holographic interferograms of investigated members subject to the geometrical form of the member investigated.

For decoding holographic interferograms we refer to expressions (1) - (6). From these expressions we see that it is necessary to determine angles θ_1, θ_2, φ_1, φ_2 defining the location of the vectors $\hat{K}_i, \hat{K}_0$ in space. Let us suppose that the aperture angle of observation is very small in comparison with the distance to the investigated point on the member. Therefore, if such a distance is selected at which the size of the investigated member on the image would be equal to the size of the imaginary image of the object reconstructed from the holographic interferogram, then it would be possible to obtain relationships which allow the calculation of the angles directly from the photograph. For this, geometrical relationships of the optical train of the holographic rig, used at the recording of this member, should be considered.

Let us consider now particular cases of the determination of angles.

The cases when the investigated member is a bar or a plate are shown in Fig. 3.

In this case, the bar is arranged in the plane of the vectors of illumination $\hat{K}_i$ and observation $\hat{K}_0$. On the rod, there is a fixed point *P* from which we start to measure the distance l to the investigated point for which the angles θ_1, θ_2 are being determined. Let us introduce an auxiliary angle

$$\gamma = arctg\left[\frac{HL}{AL_v}\right], \qquad (18)$$

where L is the length of the investigated bar determined from the image, H is the distance from the fixed point on

the surface of the plate (bar) to the considered point on the image, *A* is the distance from the fixed point on the bar to the aperture, L_n is the image of the bar (plate) at β=0.

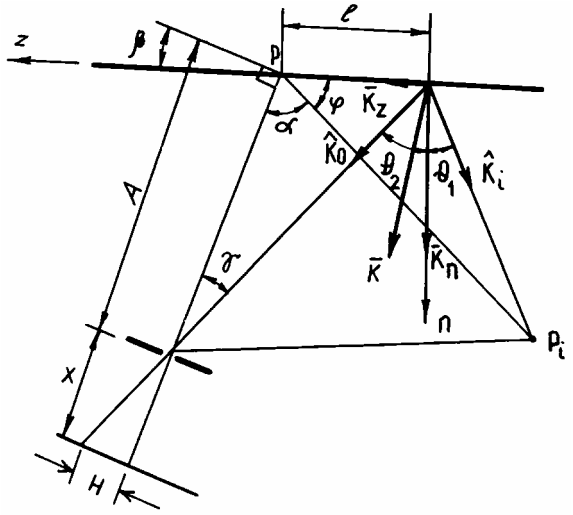

Fig. 3. **The interpretation diagram of the holographic measurement of the point lying on the bar (plate) surface; $\hat{K}$ is the sensitivity vector, $\hat{K}_i$ is the unit illumination vector of the investigated point. $\hat{K}_0$ is the unit observation vector of the investigated point, K_n, K are projections of the sensitivity vector on axes *n*, *z*, *l* is the distance from the fixed point to the aperture, *x* is the distance from the aperture to the screen, *H* is the size of the bar (plate) on the photograph, γ is the aperture angle, α is the central angle between illumination and observation directions of the investigated point**

The distance *l* from the fixed point *P* to the point considered on the bar is determined as

$$l = \frac{A\tan\gamma}{\cos(\alpha+\beta)-\sin(\alpha+\varphi)\tan\gamma}, \qquad (19)$$

where

$$tg\gamma = \frac{HL}{AL_v},$$

α is the angle between the directions of illumination and observation of the reference point *P*, which is measured from the optical holographic train and is constant; φ is the angle between the plane of the bar (plate) and the straight line PP_i, which is measured from the optical train of the holographic rig and is constant. Using the obtained relationships, the angles θ_1 and θ_2 are expressed, respectively, as

$$\theta_1 = \arctan\left[\frac{PP_i\cos\varphi - l}{PP_i\sin\varphi}\right], \qquad (20)$$

$$\theta_2 = \gamma+\alpha+\varphi-\frac{\pi}{2}. \qquad (21)$$

Here, PP_i is the distance from the illumination point to the reference point P_i on the reference point *p* on the bar (plate).

Let us analyse the case when the investigated member is a cylinder.

Consider now the cylinder which axis is located in the plane of observation $\hat{K}_0$ and illumination $\hat{K}_i$ vectors is perpendicular to the plane of the observation and illumination vectors and meets the plane of observation $\hat{K}_0$ and illumination $\hat{K}_i$ vectors at a certain angle.

Fig. 4 presents the diagram corresponding to the case when the axis of the cylinder is located in the plane of vectors of observation $\hat{K}_0$ and illumination $\hat{K}_i$. The investigated point lies on the surface of the cylinder at the distance *l* from the fixed point *p*. The angle γ can be determined from expression :

$$\gamma = \arctan\left[\frac{HL}{(A-R)L_v}\right], \qquad (22)$$

where *H* is the distance from the reference axis to the considered point on the image, L_n is the length of the image of the cylinder at β=0 (when the cylinder axis is parallel to the screen), *L* and *R* are length and the radius of the cylinder, respectively.

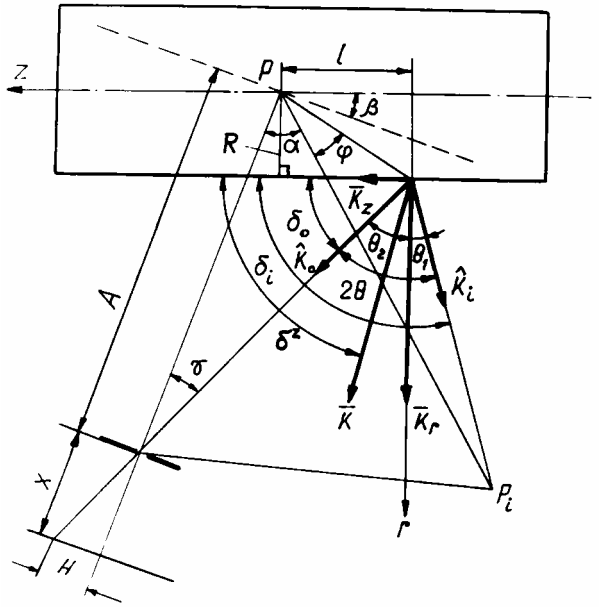

Fig. 4. **The interpretation diagram of the holographic measurement of the point lying on the surface of the cylinder for the case when the cylinder axis is located in the plane of unit vectors of illumination $\hat{K}_i$ and observation $\hat{K}_0$, $\hat{K}_r$, $\hat{K}_z$ are projections of sensitivity vector on axis *r,z* respectively, *l* is the axial distance from the investigated point on the cylinder surface to the fixed point *P*, *x* is the distance from screen to aperture, *A* is the distance from the fixed point to aperture, *R* is the radius of the cylinder, α is the angle between illumination and observation directions**

From Fig. 4 we also have:

$$l = R\tan(\alpha+\varphi-\beta) \qquad (23)$$

$$\varphi = \frac{R\sin(\alpha+\beta)-A\sin\gamma\cos(\alpha-\beta)}{R\cos(\alpha+\beta)+A\sin\gamma\cos(\alpha-\beta)} \qquad (24)$$

where PP_i is the distance from the fixed point *P* on the cylinder axis to the point of illumination P_i, which is determined experimentally from the optical circuit of the holographic rig, β is the angle defining the cylinder position relative to the observation direction and obtained experimentally from the optical train of the holographic rig, α is the central angle between the direction of observation and illumination, which is constant and is

determinable experimentally from the holographic optical train.

The angles θ_1, θ_2 for this case can be determined from expressions:

$$\theta_1 = \arctan\left[\frac{l - PP_i \sin(\alpha - \beta)}{R - PP_i \cos(\alpha - \beta)}\right], \quad (25)$$

$$\theta_2 = \gamma + \beta \quad (26)$$

Fig. 5 presents the diagram corresponding to the case when the axis of the cylinder is perpendicular to the plane of the vectors of observation and illumination.

Here we obtain the following relationships:

$$\gamma = \arctan\left[\frac{HR}{AR_v}\right] \quad (27)$$

where H is the distance from the axis of the cylinder to the point considered on the photograph, A is the distance from the axis of the cylinder to the aperture, R is the radius of the cylinder, R_i is the radius of the cylinder on the photograph.

$$\beta = \gamma + \arccos\left(\frac{A\sin\gamma}{R}\right), \quad (28)$$

$$\theta = \arctan\left[\frac{PP_t \cos(\alpha + \beta)}{R - PP_t \sin(\alpha + \beta)}\right], \quad (29)$$

$$\theta_2 = \gamma + \frac{\pi}{2} - \beta, \quad (30)$$

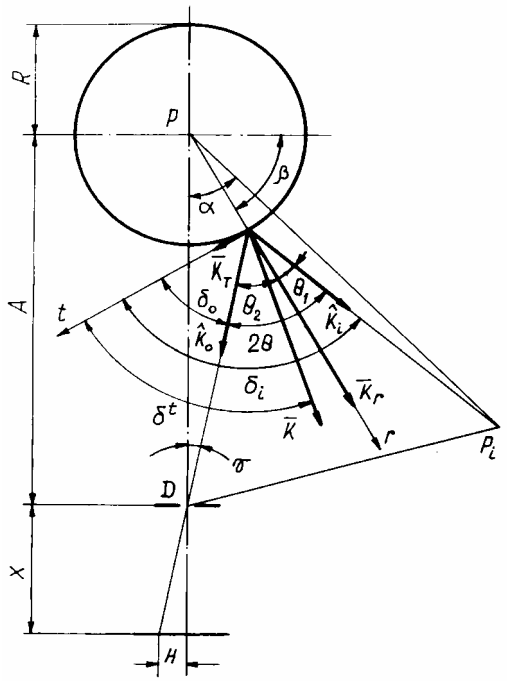

Fig. 5. **The interpretation diagram of the holographic measurement of the point lying on the surface of the cylinder for the case when the cylinder axis is perpendicular to the plane of unit illumination and observation vectors $\hat{K}$ is the sensitivity vector, $\hat{K}_r$, $\hat{K}_t$ are the projections of sensitivity vectors on axis *r, t; R* is the radius of the cylinder, *A* is the distance from the center of the cylinder *P* to the aperture, *x* is the distance from aperture *D* to screen, γ is the aperture angle**

where PP_i is the distance from the point of illumination P_i to the center of rotation of the cylinder P, β is the angle defining the coordinate of the investigated point on the surface, α is the central angle between the directions of observation and illumination determinable experimentally from the optical holographic train.

Fig. 5 presents the diagram corresponding to the case when the axis of the cylinder meets the plane of vectors of observation and illumination at an some angle. In this case, the angles φ_1 and φ_2 between the cylinder element and the vectors of illumination $\hat{K}_i$ and observation $\hat{K}_0$ are determined experimentally. Since the plane of the vectors of illumination and observation makes an angle with the axis of the cylinder, the intersection of this plane with the cylinder forms an ellipse (see Fig. 7). Correlations for the determination of angles θ_1, θ_2 for the given case are given below. From Fig. 7 we have:

$$\gamma^h = arctg\left[\frac{H^h R}{AR_v}\right], \quad (31)$$

where H^h is the distance from the axis of the cylinder to the considered point on the photograph; R is the radius representing the minor semi-axis of the ellipse $b=R$;

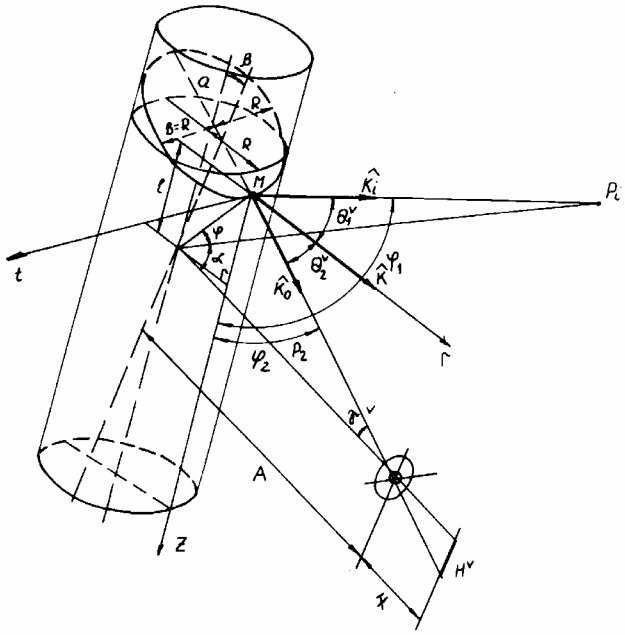

Fig. 6 **The interpretation diagram of the holographic measurement of the point lying on the cylinder surface for the case when the plane of unit illumination and observation vectors meet the cylinder axis at an angle, *R* is the cylinder radius, *y* is the major semi-axis of the ellipse, *b* is the minor semi-axis of the ellipse, *x* is the distance from aperture to screen, H^n is the position of point *M* on the photograph**

A is the distance from the axis of the cylinder to the aperture, R_n is the radius of the cylinder on the image.

The angle β defining the position of the investigated point on the ellipse can be expressed as:

$$\beta = \gamma^h + \arccos A\frac{\sin\gamma^h}{\rho}, \quad (32)$$

where r is the radius of the investigated point which is

$$\rho = \sqrt{\alpha^2 \cos^2\beta + b^2 \sin^2\beta}\,. \quad (33)$$

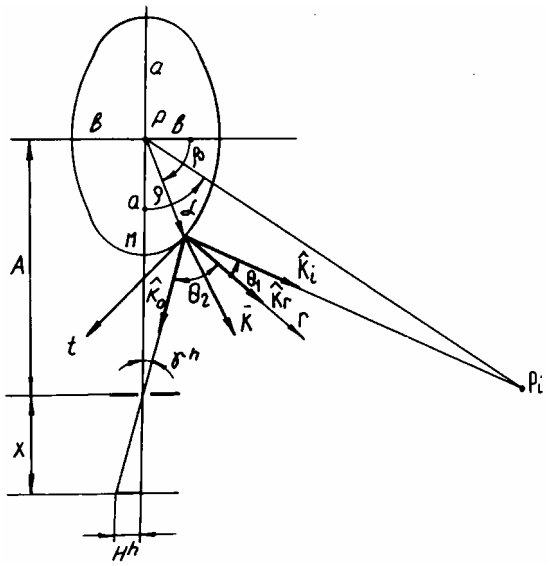

Fig. 7. **The interpretation diagram for the holographic measurement of the point lying on the cylinder surface for the case when intersection of the plane of unit vectors of illumination and observation with the cylinder axis forms an ellipse: *K* is the sensitivity vectors, K_r, K_z are the projections of sensitivity vectors on axis *r*, *t*, $\hat{K}_1$, $\hat{K}_0$ are the unit vectors of illumination and observation, *a* is the major semi-axis, *b* is the minor semi-axis, *p* is the vector of oscillations of the point, *A* is the distance from the cylinder axis to the aperture, *x* is the distance from aperture to screen, H^h is the position of the point designated by vector *p* on the photograph**

Since $\alpha = R/\cos\vartheta_2^{\nu}$ is the major semi-axis of the ellipse ($\theta^n{}_2$ is the angle between the plane of the drawing and the plane perpendicular to the axis of the cylinder), then:

$$\rho = \sqrt{\left[R^2/\left(\cos\theta_2^{\nu}\right)^2\right]\cos^2\beta + R^2\sin^2\beta}\,. \qquad (34)$$

Then the angles of illumination and observation θ_1, θ_2 will be expressed, respectively as:

$$\theta_1 = \arctan\left[\frac{PP_i\cos(\alpha+\beta)}{\rho - PP_i\sin(\alpha+\beta)}\right], \qquad (35)$$

$$\theta_2 = \gamma^h + \frac{\pi}{2} - \beta\,. \qquad (36)$$

Here, PP_i is the distance from the point P_i of illumination to the axis of the cylinder, α is the angle between the directions of illumination and observation of the point *P*, which is obtained from the optical holographic train.

Fig. 8 presents the diagram corresponding to the case when the investigated member is a sphere. The auxiliary angle α is determined by means of interactions from the expression:

$$\alpha = \arctan\left\{\frac{R_S - F}{R_S\left[1 - tg(\alpha/2)\right]}\right\}. \qquad (37)$$

Here, R_s is the radius of the sphere, *F* is equal to the distance *CT* (see Fig. 8). The angle α has to be calculated just once. In order to describe a certain point on the sphere, the angle γ_p is introduced, which is expressed as follows:

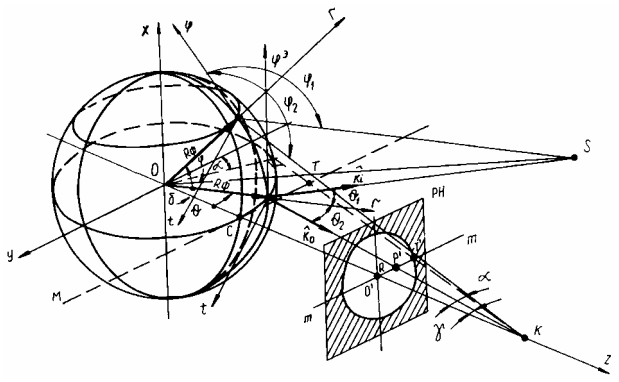

Fig. 8. **The interpretation diagram of the holographic measurement of the point lying on the sphere surface: *S* is the illumination point; *K* is the observation point, $\hat{K}_i$, $\hat{K}_0$ are the unit vectors of illumination and observation, respectively, of investigated point, R_S is the radius of the sphere, *O* is the center of the sphere, *OR* is the distance from the center of the sphere to screen, *O'T'* is the radius of the sphere on the photograph, *RP'* is the radius of the investigated point on the photograph, α is the perspective angle, γ is the aperture angle**

$$\gamma_p = \arctan\left[\frac{Rtg\alpha}{D2}\right]. \qquad (38)$$

Here, *R* corresponds in Fig. 8 to the distance *Q'P'*,defining the position of the investigated point on the photograph of the holographic interferogram, *D2* is the radius of the sphere on the photograph. It is necessary to calculate angle γ_p for each investigated point which is defined by angle θ. For the same point it is necessary to calculate angles θ and β from expressions:

$$\theta = \arcsin\left\{\left[(\alpha/R_S)+1\right]\sin\gamma_p\right\} - \gamma_p\,, \qquad (39)$$

$$\beta = \frac{\pi}{2} - \theta\,. \qquad (40)$$

The angles of illumination θ_1 and observation θ_2 are expressed, respectively, as

$$\theta_1 = \arctan\left|OS\cos(\beta+\delta)/\left[R_S - OS\sin(\beta+\delta)\right]\right|, \qquad (41)$$

$$\theta_2 = \theta + \gamma\,,$$

where *OS* is the distance from the illumination point *S* to the center of the sphere, θ is the central angle between the directions of illumination and observation, which is determined experimentally from the optical holographic train. Thus the obtained relationships allow determination of projections of the sensitivity vector directly from the holographic interferograms, depending on the optical holographic train and the geometrical form of the member of a precision mechanism.

Algorithm of calculation of the 3-D Vibrations at any point of the surface

The relation of the component of the vector of spatial vibrations with the optical scheme of the experiment is the following (see Eq. 8):

$$\frac{\lambda}{2\pi}\Omega = U(soc\varphi_1 + \cos\varphi_2) + V(\sin\theta_1\sin\varphi_1 - \sin\theta_2\sin\varphi_2) + W(\cos\theta_1\sin\varphi_1 + \cos\theta_2\sin\varphi_2). \qquad (42)$$

where l is the wavelength of the laser used to obtain the holographic interferogram, θ_1, θ_2, φ_1, φ_2 are the angles of illumination and observation that are used when recording the interferogram, W is the parameter determined from dark interferentional bands at the center of the interferogram.

By taking into account Eq. 42 for the performed m measurements we construct the system of equations

$$\begin{aligned}
&\frac{\Omega^{(1)}\lambda}{2\pi} = U^{(1)}\left(\cos\varphi_2^{(1)} + \cos\varphi_1^{(1)}\right) + V^{(1)}\left(\sin\theta_1^{(1)}\sin\varphi_1^{(1)} - \right.\\
&\left. - \sin\theta_2^{(1)}\sin\varphi_2^{(1)}\right) + \\
&+ W^{(1)}\left(\cos\theta_1^{(1)}\sin\varphi_1^{(1)} + \cos\theta_2^{(1)}\sin\varphi_2^{(1)}\right),\\
&\frac{\Omega^{(2)}\lambda}{2\pi} = U^{(2)}\left(\cos\varphi_2^{(2)} + \cos\varphi_1^{(2)}\right) + \\
&+ V^{(2)}\left(\sin\theta_1^{(2)}\sin\varphi_1^{(2)} - \sin\theta_2^{(2)}\sin\varphi_2^{(2)}\right) + \\
&+ W^{(2)}\left(\cos\theta_1^{(2)}\sin\varphi_1^{(2)} + \cos\theta_2^{(2)}\sin\varphi_2^{(2)}\right),\\
&\frac{\Omega^{(i)}\lambda}{2\pi} = U^{(i)}\left(\cos\varphi_2^{(i)} + \cos\varphi_1^{(i)}\right) + \\
&+ V^{(i)}\left(\sin\theta_1^{(i)}\sin\varphi_1^{(i)} - \sin\theta_2^{(i)}\sin\varphi_2^{(i)}\right) + \\
&+ W^{(i)}\left(\cos\theta_1^{(i)}\sin\varphi_1^{(i)} + \cos\theta_2^{(i)}\sin\varphi_2^{(i)}\right),\\
&\frac{\Omega^{(m)}\lambda}{2\pi} = U^{(m)}\left(\cos\varphi_2^{(m)} + \cos\varphi_1^{(m)}\right) + \\
&+ V^{(m)}\left(\sin\theta_1^{(m)}\sin\varphi_1^{(m)} - \sin\theta_2^{(m)}\sin\varphi_2^{(m)}\right) + \\
&+ W^{(m)}\left(\cos\theta_1^{(m)}\sin\varphi_1^{(m)} + \cos\theta_2^{(m)}\sin\varphi_2^{(m)}\right)
\end{aligned} \tag{43}$$

The components $U^{(i)}$, $V^{(i)}$, $W^{(i)}$ we express in the following way [18]:

$$\begin{aligned}
&U^{(i)} = \sum_1^q A_j^u F_{ij}^u, \qquad V^{(i)} = \sum_1^q A_j^v F_{ij}^v,\\
&W^{(i)} = \sum_1^q A_j^w F_{ij}^w,
\end{aligned} \tag{44}$$

where $U^{(i)}$, $V^{(i)}$ and $W^{(i)}$ are the corresponding tangential and normal components of the vector of spatial vibrations at the point I, $F_{ij}^U, F_{ij}^V, F_{ij}^W$ are the corresponding values of the amplitudes of vibrations at the point i of the j-th eigenmode that are calculated according to the analytical expressions. A_j^u, A_j^v, A_j^w are the influence coefficients of the j-th eigenmode.

After substitution of Eq. 44 into Eq. 43 we obtain

$$\begin{aligned}
&\frac{\Omega^{(1)}\lambda}{2\pi} = \sum_1^q A_j^u F_{1j}^u K_z^{(i)} + \sum_1^q A_j^v F_{1j}^v K_t^{(1)} + \sum_1^q A_j^w F_{1j}^w K_r^{(1)},\\
&\frac{\Omega^{(2)}\lambda}{2\pi} = \sum_1^q A_j^u F_{2j}^u K_z^{(2)} + \sum_1^q A_j^v F_{2j}^v K_t^{(2)} \sum_1^q A_j^w F_{2j}^w K_r^{(2)},\\
&\frac{\Omega^{(1)}\lambda}{2\pi} = \sum_1^q A_j^u F_{ij}^u K_z^{(i)} + \sum_1^q A_j^v F_{ij}^v K_t^{(i)} + \sum_1^q A_j^w F_{ij}^w K_r^{(i)},
\end{aligned} \tag{45}$$

$$\frac{\Omega^{(m)}\lambda}{2\pi} \sum_1^q A_j^u F_{mj}^u K_z^{(m)} + \sum_1^q A_j^v F_{mj}^v K_t^{(m)} + \sum_1^q A_j^w F_{mj}^w K_r^{(m)}.$$

In order to calculate the components of the vector of spatial vibrations at any point on the surface of the rigid body it is necessary to find the influence coefficients of the modes of eigenvibrations A_j^u, A_j^v and A_j^w. For this purpose we write the system of equations Eq. 45 in the form

$$\{W\} = [F]\{A\}, \tag{46}$$

where F is the matrix:

$$\begin{aligned}
&F[i,k] = K_z^{(i)} F_{ij}^u,\\
&F[i,q+k] = K_t^{(i)} F_{ij}^v,\\
&F[i,2q+k] = K_r^{(i)} F_{ij}^w,\\
&(i = 1,2,...m; k = 1,2...,q);
\end{aligned} \tag{47}$$

W is the column vector of dimension m,

$$\{W\} = \left\{\frac{\Omega^{(1)}}{2\pi}\lambda, \frac{\Omega^{(2)}}{2\pi}\lambda, ..., \frac{\Omega^{(m)}}{2\pi}\lambda\right\}. \tag{48}$$

We solve Eq.46 by the method of least squares, using the computer, $\{W\}$ is found from the holographic interferograms, [F] we calculate according to the analytical relationships, depending on the geometry and the conditions of fastening of the rigid body.

After the calculation of $\{A\}$ we use Eq. 46 again. We give the coordinates of any point and calculate the value of $[F]$. Because we have already calculated $\{A\}$, so after substitution of the values of $[F]$ and $\{A\}$ into Eq. 46 we calculate the components of the vector of spatial vibrations at any point of the surface.

The presented method is convenient because having several characteristic values of the vector of vibrations of the surface that are obtained from the holographic interferograms we can calculate the amplitude of the vibrations at any point of the surface of the rigid body.

Uncertainty estimation in process of numerical identification from a holographic interference pattern

Analysis of uncertainties occurring in the process of numerical identification of spatial parameters of an analysed object from its laser holographic interferogram is presented in [22]. The specific attention is devoted to the numerical identification of the centers of dark interference bands. The presented evaluation of a total uncertainty of the analysis may help to optimise the identification process and to avoid critical mistakes in the procedure for calculation of parameters of the analysed object.

Interpretation of laser holographic interferograms is a rather complicated and perplexing procedure, especially if the geometry of the analysed object is not evident. There are methodologies used for the identification of object deformations from the interference band pattern, mainly based on the recognition of the centers of interference bands [23–26]. Such methodologies give an opportunity to calculate general characteristics of spatial deformations from time averaged holograms.

The process of defining the characteristics of the dynamical system from its holographic interference pattern

is relatively heavily imposed by different sources of errors starting from uncertainties reflecting the geometric characteristics of the optical scheme, finishing with the uncertainties caused by numerical procedures for the identification of interference band centers. The process of decision making from the holographic patterns thus may be consequenced by rather high error levels. The knowledge about these errors and their ranges is quite critical in applications when the necessary precision level in to be maintained.

The proposed method of spatial deformations identification is based on the fact that steady state vibrations of a structure may be expressed as a linear mixture of natural eigenmodes . Though the calculation of weight coefficients of appropriate eigenmodes also serves as a new source of errors, such a methodology may help to understand the dynamical processes of the analysed object in a better way, and thus compensate the uncertainties originated from other sources.

The process of reconstruction of spatial deformations vector from laser optic interference hologram is schematically shown in Fig. 9.

Basically it consists of the following stages:

- Scanning and filtering the image of an optical hologram (Block 1).
- Numerical interpretation of interference bands and reconstruction of spatial deformation vector (Block 2).
- Numerical adjustment of reconstructed spatial deformation vector (Block 8).

The process of reconstruction of spatial vibrations yields the occurrence of inaccuracies which are appropriately grouped as errors originating from the numerical location of centers of interference bands (Block 3), errors associated with uncertainties of geometrical parameters of the optical system (Block 4), and errors from the approximation through the natural eigenmodes (Block 5). All uncertainties are summing up (Block 6) and forming the total uncertainty of reconstructed deformation vector (Block 7), which must be evaluated while constructing the final shape of spatial vibrations (Block 8).

Further considerations about the total uncertainty of the reconstruction require the analysis of every individual source of errors.

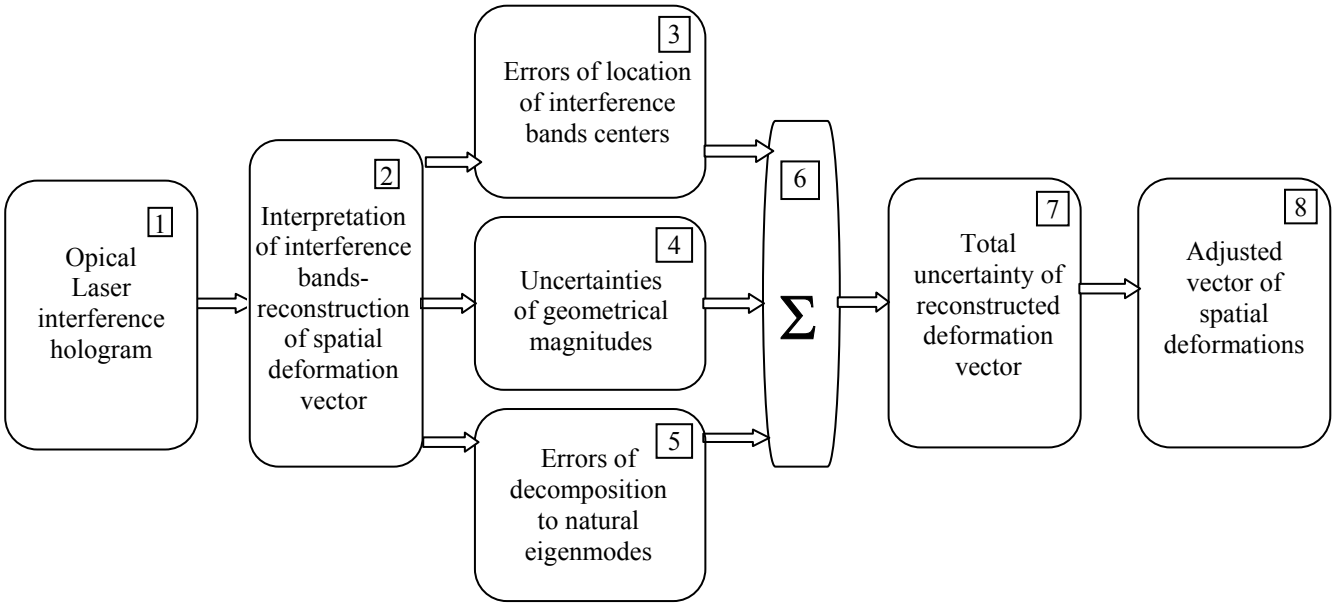

Fig. 9. **The schematic diagram of uncertainty estimation in the process of reconstruction of deformation vector from the optical interference hologram**.

The reconstruction of spatial object characteristics from its interference pattern is based on the identification of the centers of dark interference bands [23]. Thus the uncertainty of the numerical analysis procedure in principle depends on the ability of the software to determine the centers of an interference band with a predefined accuracy.

Fig. 3.3.2 present a process of identification of centers of interference bands from the measured holograms with following numerical reconstruction of bands and statistical displacement identification on the surface of the measured object.

It is obvious that the accuracy of determination of interference lines in the holograms varies from ±1,0 up to ± 3,0 mm in the zones where the angle between the illumination vector $\boldsymbol{K_i}$ and the normal vector of the surface is less than $\pi/4$. Thus, the optical phase measurement uncertainty $\delta(\Delta\Omega) \leq 0{,}3$ rad. It is apparent, that if the angle between the illumination vector and the normal vector of the surface is turning to become larger, the errors from the band identification may be sufficiently larger (Fig. 10 - bottom part of the pattern). Of course, one could not expect the original hologram to sustain a good picture quality in this region. In such a case a poor quality of the original hologram cannot lead to perfect results of the numerical analysis.

The evaluation of uncertainties of the geometrical parameters of the system requires the definition of the mathematical relationships between the illumination and sensitivity vectors. The mathematical model of the

hologram registration scheme evaluates the position of lighting and observation vectors, as well as the position of the analysed object itself. Let the illumination vector $\vec{K}_i$ and the observation vector $\vec{K}_0$ be constructed in the co-ordinate set *r, t, z* with corresponding angles θ_1, φ_1, ψ_1 and θ_2, φ_2, ψ_2. It is obvious that (see Eq. 6).

$$\begin{aligned}\vec{K}_i^{\,j} &= \cos\theta_1^j \cdot \vec{r} + \cos\varphi_1^j \cdot \vec{t} + \cos\psi_1^j \cdot \vec{z},\\ \vec{K}_0^{\,j} &= \cos\theta_2^j \cdot \vec{r} + \cos\varphi_2^j \cdot \vec{t} + \cos\psi_2^j \cdot \vec{z},\\ j &= 1,2,...,n.\end{aligned} \tag{49}$$

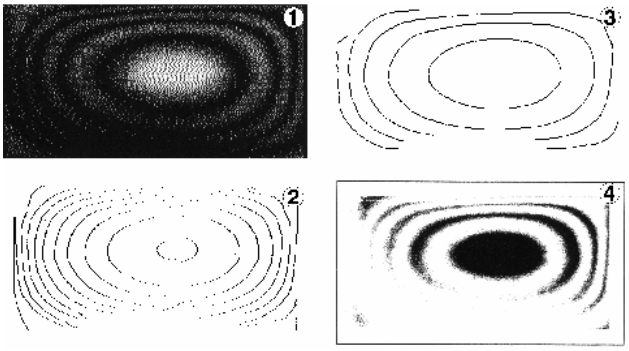

Fig. 10. **Numerical identification. (1) - Scanned and filtered hologram of an excited rectangular plate. (2) - Numerical identification of maximum and minimum values of illumination. (3) - Improved identification of maximums in the centers of interference bands. (4) - Numerical reconstruction of interference bands from the co-ordinates of maximums of interference bands**.

Now Eq. 7 can be expressed in the matrix format:

$$\frac{\lambda}{2\pi}\{\Delta\Omega\} = [K]\cdot\{R\}, \tag{50}$$

where

$$\begin{aligned}\{\Delta\Omega\} &= \{\Delta\Omega_1, \Delta\Omega_2, \Delta\Omega_3\},\\ \{R\} &= \{U, V, W\},\end{aligned} \tag{51}$$

$$[K] = \begin{bmatrix} \cos\theta_1^1 + \cos\theta_2^1 & \cos\varphi_1^1 + \cos\varphi_2^1 & \cos\psi_1^1 + \cos\psi_2^1 \\ \cos\theta_1^2 + \cos\theta_2^2 & \cos\varphi_1^2 + \cos\varphi_2^2 & \cos\psi_1^2 + \cos\psi_2^2 \\ \cos\theta_1^3 + \cos\theta_2^3 & \cos\varphi_1^3 + \cos\varphi_2^3 & \cos\psi_1^3 + \cos\psi_2^3 \end{bmatrix}.$$

Under the assumptions that the uncertainties of the components of the vibration vector are the same in all three directions:

$$|\delta U| = |\delta V| = |\delta W| = \delta\nu,$$

and therefore:

$$\delta(\Delta\Omega_1) = \delta(\Delta\Omega_2) = \delta(\Delta\Omega_3) = \delta(\Delta\Omega), \tag{52}$$

the phase uncertainty can be expressed from Eq. 51:

$$\delta\nu_{\Delta\Omega} \le \delta(\Delta\Omega)\cdot\left\|K^{-1}\right\|\cdot\lambda/2\pi, \tag{53}$$

where $\left\|K^{-1}\right\|$ is the matrix norm, i.e. the maximum radical of eigenvalue of product $\left[K^T\right]\cdot[K]$.

From Eq. 53 it is clear that the analysis of uncertainty of numerical identification of $\delta(\Delta\Omega)$ is necessary in addition to errors of geometrical parameters.

From Eq. 1 – Eq. 3 it can be seen that the phase uncertainty $\delta\nu_\Theta$ is dependant from the angles $\theta_1^j, \theta_2^j, \varphi_1^j, \varphi_2^j, \psi_1^j, \psi_2^j$ and $\delta\Theta$:

$$\delta\nu_\Theta \le \frac{\delta\Theta\cdot\left\|K^{-1}\right\|\cdot\|K_0\|\cdot\|R\|}{\sqrt{3}}, \tag{54}$$

where $\|R\|$ denotes the norm of the vector $\vec{R}$, i.e. $\|R\| = \dfrac{1}{\sqrt{U^2+V^2+W^2}}$, and

$$[K_0] = \begin{bmatrix} \sin\theta_1^1 + \sin\theta_2^1 & \sin\varphi_1^1 + \sin\varphi_2^1 & \sin\psi_1^1 + \sin\psi_2^1 \\ \sin\theta_1^2 + \sin\theta_2^2 & \sin\varphi_1^2 + \sin\varphi_2^2 & \sin\psi_1^2 + \sin\psi_2^2 \\ \sin\theta_1^3 + \sin\theta_2^3 & \sin\varphi_1^3 + \sin\varphi_2^3 & \sin\psi_1^3 + \sin\psi_2^3 \end{bmatrix}.$$

The typical experimental geometric uncertainty of the angles $\theta_1^j, \theta_2^j, \varphi_1^j, \varphi_2^j, \psi_1^j, \psi_2^j$ is usually not greater than ±0,004 rad.

Let us evaluate errors occurring in the process of decomposition of motion to natural eigenmodes. From Eq. 44 it is obvious that the identification of the natural eigenmodes F_{ij}^X, and appropriate weighting coefficients of the corresponding eigenmodes A_j^X (here $X \in \{U, V, W\}$, j varies from 1 up to the number of highest evaluated eigenmode, may originate quite serious uncertainties and impact the total uncertainty of the numerical experiment (Fig. 9). Moreover, the precise knowledge about the physical object is required for the calculation of its eigenshapes. The alternation of boundary conditions may change the shapes of natural eigenshapes in a radical way.

Nevertheless, such a methodology may help to identify the spatial deformations in case when the quality of the optical hologram is poor. In other words, losses in errors compensate the damages of the original hologram.

Fig. 10-(1) presents a scanned and filtered optical time averaged hologram of a rectangular plate, laser wave length λ = 0,63 μm. It may be noted that the bottom center area of the hologram holds a minimum useful information. This is mainly due to incorrect illumination vector position relatively to the surface of the plate. Numerical reconstruction of the centers of interference bands (Figures 10-(2)-(3)) clearly accents the problem. Straightforward identification of the spatial deformations would leave this zone undefined.

The knowledge of the physical properties of the plate (all four boundary side walls of the plate are fixed) may help to identify the spatial deformations. The equation of flexural vibrations of a plate is written in the form [27]:

$$\frac{Eh^3}{12\left(1-\nu^2\right)}\nabla^4 u + \rho_0 h\ddot{u} - f = 0, \tag{55}$$

where E is the Young's modulus, ρ_0 is the density of plate material, h is the thickness of the plate, ν is the Poisson's ratio, f is the exciting force, u is displacement of the plate.

Natural eigenmodes are sought in the form:

$$U(x,y,t)=U(x,y)e^{i\omega t}=X(x)\cdot Y(y)\cdot e^{i\omega t}, \qquad (56)$$

where t is the time, ω is the natural frequency. The approximated solution takes the following form:

$$X_n(x)=A\sin\left(\frac{n\pi}{a}\cdot x\right),$$
$$Y_m(y)=B\sin\left(\frac{m\pi}{b}\cdot y\right), \qquad (57)$$

where a, b are the plate dimensions in x and y directions, respectively, n, m are the number of half-waves in x and y directions.

The reconstruction of the first natural eigenmodes and calculation of appropriate weighting coefficients shows that the coefficient A_1 tends to unity, rest tending to zero, thus the plate's displacement vector is coinciding with motion described by Eq.57 at $n = 1$, $m = 1$.

The uncertainty of such an evaluation $\delta\nu_{XY}$ is highly dependent mainly on two factors: the accuracy of band identification and the accuracy of eigenmodes calculation. The evaluation of the second uncertainty is in its term very much dependant on the knowledge about the boundary conditions of the object. If the boundary conditions are clearly defined (as in the presented example), then

$$\delta\nu_{XY}=2\cdot\delta\nu_{\Delta\Omega} \qquad (58)$$

Total uncertainty of identification of spatial vibrations can be expressed in the following way:

$$\delta\nu=\delta\nu_{\Delta\Omega}+\delta\nu_{\Theta}+\delta\nu_{XY}, \qquad (59)$$

here all three terms of summation are defined earlier.

The validity of numerical identification of spatial vibrations from a holographic interference pattern depends on both on the geometrical and numerical uncertainties. An estimate of these uncertainties may help to avoid errors in interpreting the holographic interferograms. Moreover, application of approximation through natural eigenmodes helps to identify even those regions of the hologram which are not vivid due to technical or geometrical reasons.

The advantages of such a type of interpretation of holographic images may be clearly illustrated by the following practical example. The original hologram of a vibrating plate with left and right fixed borders (upper and bottom edges are free) is presented in Fig. 11.

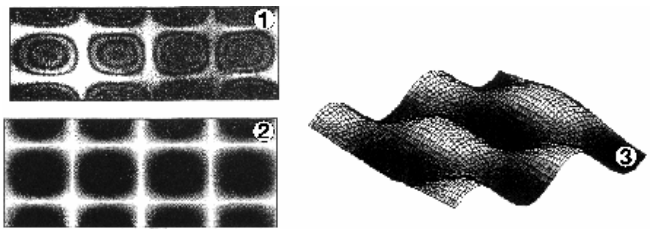

Fig. 11. **Interpretation hologram of holographic images. (1) – experimental holographic interferogram, (2) – filtered hologram, (3) – deformable surface in numerical expression**

The reconstructed motion is of a fifth eigenmode with coefficients $m = 3$, $n = 2$ (Eq. 57), coefficient $A_5 = 0{,}96$ with the uncertainty ±0,053.

The total uncertainty affecting the process of reconstruction of spatial deformation vector from optical laser interference hologram has been evaluated. Every separate source of uncertainties is considered presenting a practical example of reconstruction. A new method of approximation based on the eigenshapes of the system is presented. The analysis performed may help to get a better and more precise knowledge about the investigated models.

Conclusions

The proposed procedure and algorithm for the analysis of holographic interferograms can be used to optimize the operation of wave mechanical systems in real structures. Method is also applicable to the analysis of holographic interferograms of three-dimensional vibrations of deformable solids of any geometry of shapes. Presented methods allow to do quantitive interpretation of the interference patterns in the cases of different types of vibrations. Algorithm of calculation of components vector sensitivity according can be used for design of an automated fringes analysis system.

A system for holographic interferometry images quantitive parameter identification is developed and can be useful for the investigation for the links of different shapes. An interference bands identification algorithm is coupled with the data of geometric parameters of experimental set-up thus producing a powerful tool for object identification.

The total uncertainty affecting the process of reconstruction of spatial deformation vector from optical laser interference hologram has been evaluated.

Reconstruction of the interference fringes based on the eigenmodes increases accuracyof unwrapping fringes compared with the others methods.

References

1. **Bryanston-Cross P.J., Quan C., Funes-Gallanzi, Judge T.R.** Quantitative analysis of holographic particle data. Optics and lasers in engineering. 1993. V.18. P.267-279.
2. **Khanna S.M., Tonndorf J. et al.** Vibratory patterns examined by real-time and time-averaged holography. Journal of the acoustical society of America. 1973. 54(6). P.1686-1693.
3. **Wernice G., Gruber H.** Improvement of visual interpretation of interferograms in holographic microscopy. Physical research. fringe 89. Automatic processing of fringe patterns. W.Osten (ed.). Akademic-Verlaf, Berlin. 1989. P.154-157.
4. **Kruschke O., Wernice G., Gruber H.** Holographic interferometric microscope with conjugate reconstruction for the determination of three-dimensional displacements. Optical Engineering. 1996. 34(4). P.1122-1127.
5. **Shibaymma K., Uchiyama H.** Measurements of three-dimentional displacement by hologram interferometry. Applied optics. 1971. V.10. P.2150.
6. **Wernice G., Kruschke O., Huth T., Demoli N., Gruber H.** Evaluation of deformation vectors in holographic interferometric microscopy with conjugated reconstruction. Holographic and diffractive techniques. Berlin, G.Dausmann (ed.), SPIE - Proc. 1996. 2951. P.47-56.
7. **Bryanston-Cross P.J., Quan C., Funes-Gallanzi, Judge T.R.** Quantitative analysis of holographic particle data. Optics and lasers in engineering. 1993.18. P. 267-279.
8. **Kowalevski G.** 3D shock wave phenomena visualised with holographic interferometry. Proceedings SPIE 2513, 21st International congress on high speed photography and photonics. Teajon, Korea. 1995. P. 947-959.

9. **Hustad C.W., Squire L.C.** Application of holographic interferometry for evaluation of 3D navier-stokes calculations. Experiments in fluids, Springer-Verlag. 1995. Vol.18. P. 343-350.
10. **Monteiro J., Vaz M.A.P., de Melo F.Q., Gomes J.F.S.** Use of interferometric techniques for measuring the displacement field in the plane of a part-through crack existing in a plate. 15th Symposium Danubia-Adria on experimental methods in solid mechanics. Bertinoro, Italy, 30th of September a 3 October, 1998.
11. **Shibaymma K., Uchiyama H.** Measurements of three-dimentional displacement by hologram interferometry. Applied optics. 1971. Vol.10. P.2150.
12. **Palevičius A., Ragulskis M.** Holographic interference method for investigation of wave transport systems. Proceedings of the International society for optical engineering. 1996. Vol. 2868. P.225-231.
13. **Palevičius A.** Calculation 3-D Vibrations by the holographic interferograms. Proceedings International seminar wave mechanical systems. Kaunas: Tecnologija. 1996. P.8-11.
14. **Palevičius A., Ragulskis M.** The system of wave transformation holographic research. Proceedings of the International society for optical engineering. 1998. Vol.3411. P.125-128.
15. **Palevičius A., Ragulskis M.** Considerations about chaotic dynamics of exhaust tube and its design optimization in respect to its dynamic properties. Proceedings SAE of the 1999 noise and vibration conference. 1999. Vol. 1. P.59-63.
16. **Palevičius A., Ragulskis K., Vasiliauskas R.** Calculation of sensitivity vector projections from photographs of holographic interferograms when interpreting tree-dimensional oscillations. Vibration engineering. 1988. Vol.2. P.373-383.
17. **Vasiliauskas R., Palevičius A., Ragulskis K**. Analysis of holographic interferograms by ultrasonis piezoelectric transducers in the investigation of three-dimensional vibrations. Acoustical physics. 1988. 34(6). P.573-575.
18. **Gontkevich V.S.** Normal modes vibration of plates and shells. Handbook (in Russian), Naukova Dumka, Kiev, 1964.
19. **Vest C.M.** Holography interferometry. Willy, New York, 1979.
20. **Stetson K.A., Molin N.E.** Measuring combination mode vibration patterns by hologram interferometry. Journal of scientific instruments. 1969
21. **Tonin R., Bres D.** Journal optic soc.am. 1978. Vol. 68. P.924.
22. **Ragulskis M., Palevičius R., Ragulskis L., Palevičius A.** Uncertainty estimation in the process of numerical identification of spatial vibrations from holographic interference patterns. Informacinės technologijos ir valdymas. 1999. Vol. 4(13). P.47-51; Informacinės technologijos ir valdymas. 2000, Vol.2(15). P.45-49.
23. **Cloud G.L.** Optical methods of engineering analysis. SEM. 1998. P.503.
24. **Iwatsuki N., Hayaschi I., Kitagawa.** The measuring accuracy of a laser speckle interferometry using a double-aperture method. Intl. J. Japan soc. prec. eng. 1994. Vol. 28(2). P.156-163.
25. **Rost R., Deblauwe E.** A parameter estimation algorithm for spatial sine testing. Intl. J. of analytical and experimental modal analysis. 1992. Vol. 7(3). P.213-226.
26. **Vanlanduit S., Guillaume P.** Development of data reduction procedure with noise extraction for high spatial resolution optical measurements. Proceedings SPIE, Italy. 1998. P.357-362.
27. Вибрации в технике. Справочник: в 6-тит, Москва: “Наука” 1978-1981.

A. Palevičius

Suvidurkintų laike holografinių interferogramų trimačių virpesių kiekybinio įvertinimo teorija

Reziume

Straipsnyje pateikiama metodika kietų deformuojamų kūnų paviršiaus virpesio vektoriaus normalinei ir tangentinėms dedamosioms apskaičiuoti pagal holografines interferogramas. Nagrinėjami atvejai, kai deformuojamas kūnas yra strypas, plokštelė, cilindras arba sfera.

Pateikta interferogramų analizės teorija leidžia kiekybiškai įvertinti harmoniniu dėsniu aprašomas mechanines sistemas, kurių darbas pagrįstas grandžių virpėjimu ultragarsinių dažnių juostoje.

Pateikta spaudai: 2001 03 12

DOI: 10.5755/j01.u.38.1.8041